AIAA JOURNAL
Vol. 38, No. 10, October 2000

Structural Optimization Using Computational Aerodynamics

Daniella E. Raveh,* Yuval Levy,† and Moti Karpel‡
Technion—Israel Institute of Technology, Haifa 32000, Israel

A recently developed methodology for aircraft structural design, based on nonlinear airloads, is extended to include a modal-based optimization option and is employed with a new computational aerodynamics code for loads analysis. Nonlinear maneuver loads are evaluated by a computational scheme that efficiently combines fluid dynamics iterations with iterations for elastic shape deformations and trim corrections. An efficient design process is obtained by performing several structural optimization runs during one maneuver load analysis, where each optimization is based on the interim nonconverged airloads. To allow for the efficient application of the method with large finite element structural models and many constraints, the discrete-coordinate optimization scheme is replaced by a modal-based optimization where a set of low-frequency vibration modes of the baseline structure is used to represent the structure throughout the optimization, both for response analysis and for sensitivity analysis. Comparative modal-based and discrete-coordinate design cases are shown to converge to the same optimal design variable values, even though they do not follow the same path. Two flow solvers are used, one of which is a newly developed Euler/Navier–Stokes computational aerodynamics code that is capable of handling complex geometries by using the Chimera overset grid method. The method avoids the problem of mesh discontinuities due to elastic shape deformations and control surface deflections because the displacements of each component affect only the component's mesh. The method is demonstrated with a wing–fuselage–elevator transport aircraft model performing symmetric and antisymmetric maneuvers at Mach 0.85.

Introduction

A MAIN issue in structural design optimization is the validity of the disciplinary analyses used, especially the structural analysis and the fluid dynamics analysis. Evidence of this can be found in structural design studies based on very detailed finite element models.[1] In contrast, aerodynamic tools of automated structural design systems, for example, NASTRAN[2] and ASTROS,[3] are usually based on the relatively simple linear potential flow models, for example, the doublet-lattice method.[4] Whereas linear aerodynamics provides a good approximation of the aerodynamic loads in the subsonic flow regime, it may be inadequate for the transonic regime, where shock waves significantly affect the flowfield. In the more advanced stages of structural design, the linear aerodynamic loads are normally replaced with more accurate maneuver loads, calculated from databases of loads from wind-tunnel testing or from computational fluid dynamics (CFD) analyses; for example, see Ref. 5. These databases reflect the airloads acting on the rigid configuration and, thus, have to be corrected to account for structural elasticity.

Three major obstacles prohibit the use of CFD schemes for structural design: First, regular CFD schemes are designed to provide the airloads on a rigid configuration, in specific flight conditions. They do not have the required mechanism to account for aircraft flexibility and required algorithms to trim the aircraft angle of attack and control surface deflections according to the prescribed maneuvers required for structural designs. Second, high computational costs are associated with CFD analyses. This difficulty is amplified in structural design applications where the airloads have to be evaluated several times during the design process. Third, aeroelastic considerations require the evaluation of the derivatives of the aerodynamic loads with respect to the structural design variables. When using nonlinear CFD analyses, these derivatives are not available explicitly, and their evaluations by finite-difference methods typically amount to unreasonable computational costs.

Several studies published in recent years address the evaluation of maneuver loads using CFD schemes. Generally, these studies differ in the CFD scheme used, the structural elastic model, the way the two disciplines are integrated, and the amount of generality and complexity of the studied test cases. The early works on computational static aeroelasticity combined CFD analyses with simple structural models and were applied to wing models only.[6–8] Tatum and Giles[9] addressed a complete aircraft configuration using a full potential aerodynamic method (SIMP), together with an equivalent plate structural model, and Vinh et al.[10] added a trim routine to the CAP-TSD code.[11] Schuster et al.[12] addressed the problem of computing the flowfield about flexible fighter aircraft operating at extreme flight conditions, using Euler/Navier–Stokes simulations for flows where the small disturbance assumption is no longer valid. Guruswamy,[13] Guruswamy and Byun,[14] Appa et al.,[15] Kapania et al.,[16] Guruswamy and Tu,[17] and Byun and Guruswamy[18] performed aeroelastic computations on a wing, a wing–fuselage configuration, and complete aircraft configurations using an Euler/Navier–Stokes aerodynamic method coupled with finite element structural models (ENSAERO).

Karpel et al.[19] introduced an efficient computational scheme for evaluating the aerodynamic maneuver loads on flexible rockets in supersonic flight conditions, based on an Euler solver. Computational efficiency was obtained by applying a relatively small number of elastic shape updates and maneuver trim corrections during the process of flowfield convergence. This scheme was expanded by Raveh et al.[20] to realistic aircraft configurations whose trimmed conditions were achieved through the use of varied incidences, control surface deflections, and rotation rates. A modal structural model was used for interfacing the CFD and structural models and for calculating elastic shape deformations and applying them to the CFD grid. A trim-correction algorithm was used for varying the incidences and control-surface deflections for obtaining user-defined maneuvers. This maneuver loads scheme serves also in the current study.

Raveh and Karpel[21] introduced a structural design methodology based on nonlinear maneuver loads. An affordable design process, in terms of the required computational resources, is obtained by a new approach to the integration of analysis and optimization. Several structural optimization runs, using ASTROS, are performed within one flow simulation, where each optimization run is based on interim, nonconverged maneuver loads, such that the flow simulation and the structural design are converged simultaneously. The necessity of computing the sensitivity of the airloads to structural design changes is circumvented because in every optimization run the airloads are applied as a fixed set of loads. The number of iterations required for convergence of the combined maneuver-optimization

Received 13 September 1999; revision received 25 February 2000; accepted for publication 11 March 2000.

*Graduate Student, Faculty of Aerospace Engineering; currently Postdoctoral Fellow, School of Aerospace Engineering, Georgia Institute of Technology, Atlanta, GA 30332-0150.

†Senior Lecturer, Faculty of Aerospace Engineering.

‡Professor, Faculty of Aerospace Engineering.

analysis is practically the same as that of regular CFD analysis for a rigid-shape configuration.

The preceding approach is based on the assumption that the computational time required for structural optimization is relatively small compared to the time required for the CFD loads analysis. For large finite element models, and for design studies that involve many constraints, this assumption may not be valid. The current study broadens the design methodology of Ref. 21 to include the modal-based option to structural optimization, as presented by Karpel and Brainin[22] and Karpel et al.[23] The modal-based structural design is based on modal representation of the structure in both the static and the dynamic disciplines. The structure is represented throughout the optimization by a set of the low-frequency vibration modes of the baseline structure. The disciplinary responses and their sensitivity derivatives to changes in the design variables are calculated with respect to the modal coordinates. The reduced-basis modal representation decreases the computational cost of typical design cases by one to two orders of magnitude.[22,23]

The purpose of the current study is to integrate CFD-based maneuver loads into a structural design optimization scheme that accounts for stresses and static aeroelastic considerations. In contrast to the traditional design process, the current study presents a fully automated integration of the load analysis and the design steps, such that the optimization is based on the computed, nonlinear, trimmed loads, and the loads computation is automatically affected by the structural changes during the design process. The modal-based structural optimization approach is integrated to provide an afordable design approach for design of realistic aircraft that are based on comprehensive models.

The computation of maneuver loads in Refs. 20 and 21 is also generalized in this study to include a different CFD scheme that is more suitable for applications that involve moving grids. Comparison of maneuver loads analyses performed with the two different CFD schemes demonstrates the independence of the algorithms with respect to the CFD method used.

Maneuver Loads Analysis

Maneuver load analysis comprises three levels of iterative processes. The innermost level contains the original CFD analysis for a rigid-shape configuration, which, if iterated until convergence, provides the aerodynamic load distribution on the rigid aircraft with prescribed aerodynamic incidences. The next iterative level introduces the structural elasticity, which is combined with the aerodynamic loading to obtain the corresponding deformed shape. This level, if iterated until convergence, provides a load distribution that agrees with that of the elastic aircraft. The outermost level contains the maneuver trim loop where the incidences and control surface deflection angles are varied to obtain the total aerodynamic forces and moments implied by the maneuver. For computational efficiency, both the elastic deformations and trim corrections are introduced during the CFD solution convergence, as shown in Fig. 1. Figure 1 contains an additional outer loop, of the structural design, which is discussed in the next section.

The user prescribes a number of CFD iterations, after which elastic deformations are computed and applied to the CFD grid, and a number of elastic shape updates, after which maneuver corrections are performed. Typically, the number of CFD iterations between two successive shape updates is 5–10% of the number of iterations required for flowfield convergence. The shape and trim parameters are not updated after each CFD iteration to avoid excessive computations and also to avoid numerical instabilities in the flow computations. The main advantages of the integrated aeroelastic computational scheme are that typical convergence rates and computational costs are very similar to those of a rigid-shape CFD run.

The core of the maneuver loads analysis is a CFD code by Yaniv[24] (FA3DMB) for solving the Euler equations. The code is based on the Jameson et al.[25] multistage method, a finite volume method using central differencing in space with explicit time stepping. A steady-state solution of the time-dependent Euler equations is obtained by iterating in time using local time steps and implicit residual smoothing.

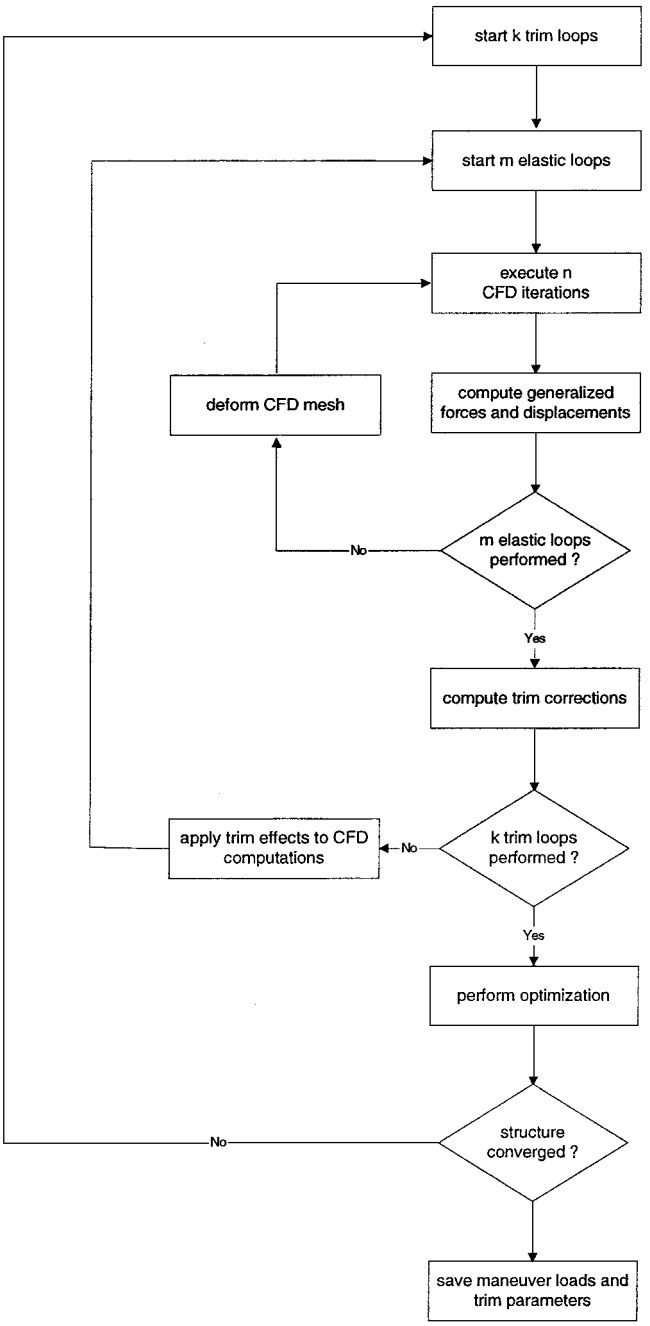

Fig. 1 Phases of the load analysis–structural optimization procedure.

Elastic shape deformations $\{u_E\}$ are calculated based on the modal approach to static aeroelasticity,[26] which assumes that the elastic deformations of the aircraft structure, under external loads, can be described as a linear combination of a set of low-frequency elastic mode shapes $[\phi_E]$, namely,

$$\{u_E\} = [\phi_E]\{\xi_E\} \tag{1}$$

where $\{\xi_E\}$ is the generalized elastic displacement vector. The static equilibrium equation in generalized coordinates is given by

$$[K_E]\{\xi_E\} = \{F_E\} \tag{2}$$

where $[K_E]$ is the generalized stiffness matrix associated with $[\phi_E]$ and $\{F_E\}$ is the generalized aerodynamic force vector. Orthogonality of the rigid-body and elastic modes with respect to the structural mass and stiffness matrices implies that $[K_E]$ is diagonal and that inertia relief effects in the right-hand side of Eq. (2) are handled

automatically.[27] The generalized forces in Eq. (2) are obtained by summing the aerodynamic forces according to

$$\{F_E\} = [\phi_{EA}]^T \{F_A(a, \xi_E)\} \tag{3}$$

where $\{F_A\}$ is the aerodynamic force vector at the aerodynamic surface grid points. The vector $\{F_A\}$ depends on the aerodynamic trim parameters vector $\{a\}$ and on the elastic shape $\{\xi_E\}$. Matrix $[\phi_{EA}]$ is the elastic modes matrix, expressed at the aerodynamic interface grid points. The elastic mode shapes are mapped from the finite elements nodes, in which they are generated, onto the CFD interface grid points, by a newly developed method, based on the infinite plate spline by Harder and Desmarais[28] and beam spline[2] methods. The interface method is presented in detail in Ref. 29.

The generalized elastic deformations are transformed into displacements of the CFD interface points and applied to the whole grid using a three steps shearing method, following the method suggested by Schuster et al.[12] First the interface points are moved, according to the computed generalized displacements, by

$$\{u_A\} = [\phi_{EA}]\{\xi_E\} \tag{4}$$

Then the surfaces ahead, behind, and beside the deformed interface surfaces are adjusted so that they meet the displaced boundaries of the interface surfaces. Finally, internal grid points are redistributed, such that each grid point along an η grid line (normal to the surface) is moved in the same direction as the first point (point $j = 1$) by the distance

$$u_j = u_1(1 - S_j/S_{gl}) \tag{5}$$

where S_j is the arc length between the j grid point and the last grid point on the grid line and S_{gl} is the total arc length of a grid line. Figure 2 shows the just-described steps of applying the elastic shape deformations to the CFD grid.

Most structural design cases are based on aerodynamic loads of prescribed aircraft steady maneuvers defined by the rigid-body accelerations $\{\ddot{\xi}_R\}$. In symmetric maneuvers, the required aerodynamic lift and moment coefficients, C_L and C_M, are related to $\{\ddot{\xi}_R\}$ by

$$qS \begin{Bmatrix} C_L \\ C_M \bar{c} \end{Bmatrix}_{\text{req}} = [M_R]\{\ddot{\xi}_R\} \tag{6}$$

where $\bar{c}$ is the reference chord, S is the reference area, and q is the dynamic pressure. The mass matrix $[M_R]$ is associated with the rigid-body modes matrix $[\phi_R]$, where the first mode reflects a unit heave and the second reflects a unit pitch about the center of gravity. Similar expressions can be written for antisymmetric or asymmetric maneuvers.

The CFD run starts with an initial estimate of the trim variables that are updated during the flowfield convergence according to the differences between the required and the current values of the aerodynamic coefficients. The current values are calculated during the CFD solution by

$$\begin{Bmatrix} C_L \\ C_M \bar{c} \end{Bmatrix}_{\text{cur}} = \frac{1}{qS}[\phi_{ER}]^T \{F_A\} \tag{7}$$

where $[\phi_{ER}]$ is the matrix of rigid-body modes expressed in the CFD surface interface points. The angle of attack α and elevator deflection δ are corrected in a symmetric maneuver by

$$\begin{Bmatrix} \alpha \\ \delta \end{Bmatrix}_{\text{new}} = \begin{Bmatrix} \alpha \\ \delta \end{Bmatrix} + \begin{Bmatrix} \Delta\alpha \\ \Delta\delta \end{Bmatrix} \tag{8}$$

where

$$\begin{Bmatrix} \Delta\alpha \\ \Delta\delta \end{Bmatrix} = \begin{bmatrix} \tilde{C}_{L\alpha} & \tilde{C}_{L\delta} \\ \tilde{C}_{M\alpha}\bar{c} & \tilde{C}_{M\delta}\bar{c} \end{bmatrix}^{-1} \left(\begin{Bmatrix} C_L \\ C_M \bar{c} \end{Bmatrix}_{\text{req}} - \begin{Bmatrix} C_L \\ C_M \bar{c} \end{Bmatrix}_{\text{cur}} \right) \tag{9}$$

and $\tilde{C}_{L\alpha}$, $\tilde{C}_{M\alpha}$, $\tilde{C}_{L\delta}$, and $\tilde{C}_{M\delta}$ are the derivatives of the aerodynamic coefficients with respect to the symmetric trim variables. With nonlinear CFD analysis, these derivatives are not available explicitly. They can be obtained from a computationally expensive finite difference analysis, but this is not necessary because trim convergence is likely to occur even with rough estimates of the derivatives. In this study, trim analysis is based on linear aerodynamic derivatives obtained from a linear analysis. Relaxation can be used to avoid large overshoots of the correcting terms, as suggested in Ref. 21.

The initial values of the aerodynamic trim parameters can be the maneuver trim parameters obtained from trim analysis conducted with linear aerodynamics. However, as shown in Ref. 21, the algorithm is robust with respect to the initial choice of trim parameters. Therefore, initial trim parameters can be almost arbitrarily set, for example, zero angle of attack and zero control-surface deflection.

Angular rates associated with the maneuver, for example, pitch rate in the symmetric maneuver case, are introduced to the aerodynamic analysis by adding terms to the fluid dynamics equations to account for them being written in a rotating frame of reference. The formulation of the flow equations in a frame of reference rotating in a steady pitch rate is presented in Ref. 29.

Following every trim iteration, the corrections to the angle of attack and control-surface deflection angle are introduced into the CFD solver. The change in the angle of attack is introduced to the CFD solver by changing the far-field flow conditions.

Changing the control-surface deflection angle amounts to a change in the configuration and, therefore, requires regeneration of the aerodynamic grid. A difficulty that arises is the slope discontinuity that is caused by the rigid rotation of the elevator relative to the fuselage, which in turn results in discontinuities in the updated CFD mesh. To avoid grid discontinuities, which are prohibited in the FA3DMB code, elevator rotations are treated by an elevator mode enhanced with a blended zone. The elevator mode is an artificial mode that describes unit rigid elevator rotation where the elevator is rigidly rotated while the rest of the aircraft does not move. Discontinuities in the mode shape are avoided by adding a blended zone at the elevator root, ranging along a few grid lines, that are moved only by a fraction of the total elevator rotation. Figure 3 shows a part of the elevator mode, where the blended zone ranges along the first two elevator grid lines. The elevator mode is used for CFD mesh update in the same way as the elastic modes are used for CFD mesh updates for elastic corrections. A different approach to avoid grid

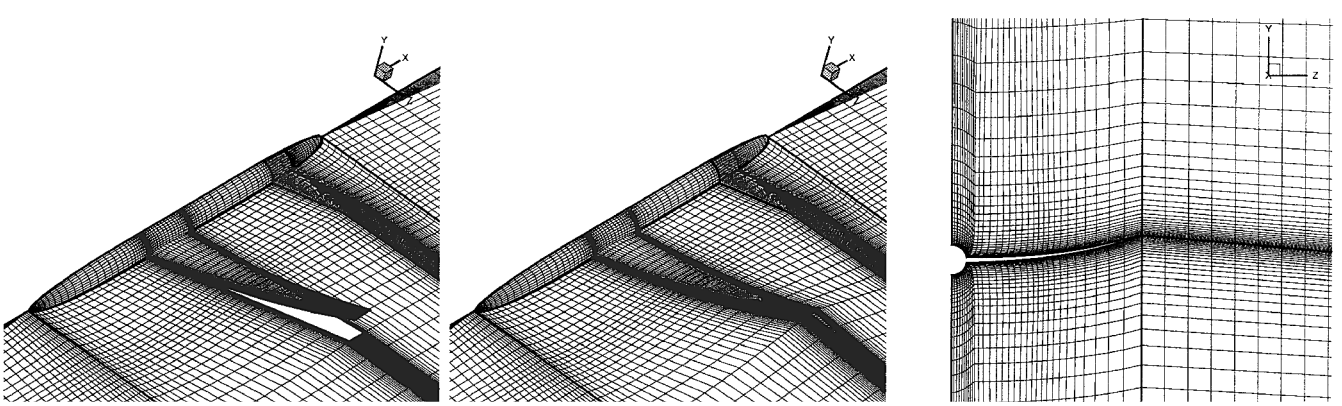

Fig. 2 Steps in the deformation of the CFD grid.

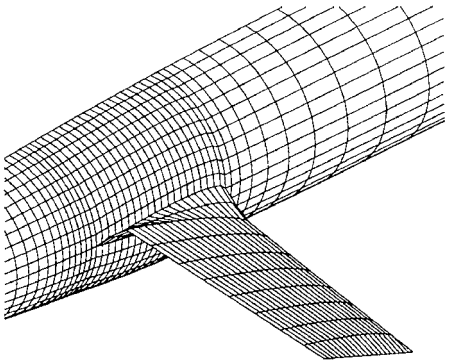

Fig. 3 Elevator mode.

discontinuities can be to create a tail mode that includes a blending zone at the fuselage grid, that is, a zone in which the fuselage grid is remeshed to coincide with the root of the deflected elevator.

This difficulty of grid discontinuities, related to relative movements of parts of the aircraft, can be avoided by using the Chimera overset grid method instead of the multiblock, patched grid approach. In this study, a similar maneuver trim procedure was introduced into a different Euler/Navier–Stokes code that employs the Chimera overset grid method.[30] The EZNSS code, developed by Levy, provides the choice between two implicit algorithms, the Beam and Warming[31] algorithm or the partially flux-vector splitting algorithm reported by Steger et al.[32] A structured computational mesh is used together with finite differences discretization method. Grid generation and intergrid connectivity are handled in the following manner. A separate computational mesh is generated for each component. An outer grid, or in the case of an aircraft, the fuselage mesh, is extended to include fully the meshes of the rest of the components. The holes that the meshes introduce into each other and the boundaries of the meshes and the holes are handled using the Chimera approach.[30] In this approach, intersecting components, such as the fuselage and the wing, create overlapping holes and, therefore, introduce complication in the intersection region. A convenient means to provide proper interpolation near intersection regions is to generate collar grids.[33] In the current work, an automatic collar grid generation for intersecting geometries is employed. The collar grid is algebraically generated based on the surfaces of the geometries and is smoothed using an elliptic grid generation method. The automatic collar grid generation is embedded in the CFD code to facilitate control-surface deflections. Also embedded in the CFD code are the hole generation and the grid connectivity procedures.

The introduction of the maneuver trim procedure into the EZNSS code allows to handle the geometry changes elegantly and removes the problems of grid discontinuities altogether. Furthermore, it demonstrates that the algorithms for elastic shape updates and trim corrections are independent of the CFD code used.

Structural Design

The main difficulty in the integration of the maneuver loads computations with structural optimization arises because the load analysis is computationally intensive and, therefore, extremely expensive. Typical time measures for the CFD and finite element models of this study are 7 h for a maneuver load analysis (on a Silicon Graphics Power Challenge using three R10000 CPUs) compared to 5 min for a structural optimization. Obviously, it is impractical to perform a complete maneuver load analysis for every optimization step.

The new approach is based on the execution of several optimization runs during the maneuver analysis, where each optimization is based on the nonconverged maneuver loads. The steps of the combined load-optimization analysis are shown in Fig. 1. The analysis starts with load computation for the baseline structure represented by its modal model. The analysis pauses several times during the flowfield convergence for structural optimization. At each pause the interim nonconverged loads are extracted and mapped onto the structural nodes. Optimization is then performed using ASTROS, while introducing the nonlinear loads as a virtually fixed set of loads. These loads do not provide the exact required maneuver loads because they are extracted from a nonconverged maneuver analysis and because of the weight changes during the optimization, which change the required maneuver lift. Therefore, at each optimization step the aircraft is trimmed using the linear rigid derivatives of the aerodynamic coefficients. These trim corrections are reduced to zero as the maneuver analysis and the structural optimization converge.

The nonlinear trimmed loads define some of the design cases in a structural optimization task. Other design cases in the same optimization task may include linear or nonlinear loads, possibly from other disciplines, and using different boundary conditions. A new modal database for the new structure is created at the final-analysis stage of the optimization. The new vibration frequencies and modes of the optimized structure are used as input to the CFD simulation, which then resumes by applying the airloads to the new structure.

Trim corrections are computed within ASTROS, based on the linear rigid aerodynamic derivatives, according to

$$\begin{bmatrix} K_{ll} & K_{lr} & -qT_{AS_l}^T A_a \\ K_{rl} & K_{rr} & -qT_{AS_r}^T A_a \\ D^T M_{ll} + M_{rl} & D^T M_{lr} + M_{rr} & 0 \end{bmatrix} \begin{Bmatrix} u_l \\ u_r \\ \Delta a \end{Bmatrix} = \begin{Bmatrix} F_{S_l} \\ F_{S_r} \\ 0 \end{Bmatrix} + \begin{Bmatrix} M_{ll} D + M_{lr} \\ M_{rl} D + M_{rr} \\ 0 \end{Bmatrix} \{\ddot{\xi}_R\} \tag{10}$$

This equation is a modified version of the trim equation solved in ASTROS,[34] where K and M are the discrete coordinate structural stiffness matrix and mass matrix, respectively. The subscripts r and l are the restrained and leftover degrees of freedom, respectively. D is the kinematic rigid-body displacement matrix, q is the dynamic pressure, $[T_{AS}]$ is the structure-to-aerodynamic model transformation matrix, $[A_a]$ is the aerodynamic force coefficient matrix for a rigid aircraft, and $\{a\}$ is the aerodynamic trim parameters vector. $\{F_S\}$ is the nonlinear maneuver loads vector, as extracted from the nonconverged CFD simulation, mapped onto the structural nodes. Equation (10) is solved for $\{\Delta a\}$, the required corrections to the aerodynamic trim parameters that would provide the maneuver rigid-body accelerations $\{\ddot{\xi}_R\}$. The equation is also solved for the l-set and r-set maneuver displacements, u_l and u_r, respectively.

ASTROS is unique in its capability to optimize simultaneously for several design cases from different disciplines with different boundary conditions. When some of the design cases require the evaluation of aerodynamic loads, the designer can choose either to perform every aerodynamic load evaluation by a separate CFD run or to limit the use of CFD only to design cases that would benefit the most from an accurate evaluation of the aerodynamic loads. When required, several CFD runs can be performed at the same time in parallel, all paused at the same position for elastic, trim, and optimization updates.

Modal-Based Optimization

The design approach presented in the preceding section was motivated by the run-time differences between an optimization run and a CFD analysis that were obtained for the models of this study. However, it is realized that for larger finite element models, and for design studies that involve a large number of constraints, the optimization run time may become much larger, and it would be impractical to perform several optimization runs within one converged CFD analysis. The computational cost of the structural optimization can be minimized, even for large finite element models, by replacing the discrete coordinates optimization with a modal-based optimization.

The basic assumption behind the modal-based optimization is the same one that is used for maneuver load analysis. The displacements calculated by Eq. (1) as a linear combination of a set of low-frequency vibration modes are used for aerodynamic load calculations and for stress analysis. It was previously shown[23] that, with approximately 20–40 modes taken into account, typical application of the basic modal approach yields accurate stress results when applied to the structure for which the modes are calculated, but exhibit large errors when applied to modified structures without changing the modal basis. To allow for an efficient, fixed-basis, optimization process with analytic sensitivity expressions,

the modal basis is complemented with modal perturbations that are calculated once for the baseline structure and then used efficiently throughout the optimization process. The revised method presented several cost-effectiveness tradeoff options. The fastest option was the first-order mode-displacement (MD) method,[35] which is also the least accurate (but still adequate in cases of moderate design changes). The summation-of-forces (SOF) method, with expandable modal basis,[23] was the most accurate option but also the most time consuming. Demonstrated with optimization cases of 5000–28,000 degrees of freedom, the various modal-based options demonstrated CPU speed-up factors of 7–80.

As will be demonstrated, the most simple modal-based optimization option (first-order MD option) can be adequately used in the CFD-based optimization process. With the modal database updated in each optimization run, the entire process should converge to the optimal solution even though the interim optimization runs might be somewhat inaccurate.

Numerical Example

Aircraft Model

A simple transport aircraft model that has all of the features necessary to verify the proposed methodology was created. The model aircraft includes a fuselage, wing, aileron, and all-movable tail. The wing and elevator are similar in shape and structure: Both are tapered and swept aft. The cross section of the wing and elevator are scaled NACA0012 symmetric airfoils. The fuselage is axisymmetric and is 20 m long. Table 1 summarizes the wing and tail geometrical dimensions.

The maneuver-load analysis and structural design described next are based on the FA3DMB code.

An H-type grid topology is used to generate the computational mesh for the flow simulations. When the multizone capability of the FA3DMB code is taken advantage of, the grid is divided into 24 zones, each describing a logical component such as wing upper/lower surface, fuselage, etc. The entire flowfield contains approximately 500,000 grid points.[21]

A general view of the structural model is given in Fig. 4. It has approximately 1000 degrees of freedom. The torsion boxes of the wing and tail and the aileron are modeled in detail with elements representing skin, ribs, spars, spar caps, and stringers. Table 2 summarizes the weights of the half-aircraft model. The wing weighs 384.6 kg of which 284.6 kg is the weight of the torsion box structure, which is subjected to optimization. A modal analysis is performed to provide the 13 low-frequency elastic vibration modes and the corresponding generalized stiffness matrix required for the CFD maneuver analysis.

Table 1 Wing and tail geometrical dimensions

Parameter	Wing	Tail
Aspect ratio	10	6.4
Half span, m	10	4
Root chord, m	3	1.5
Leading-edge sweep angle, deg	20	20
Taper ratio	0.333	0.667

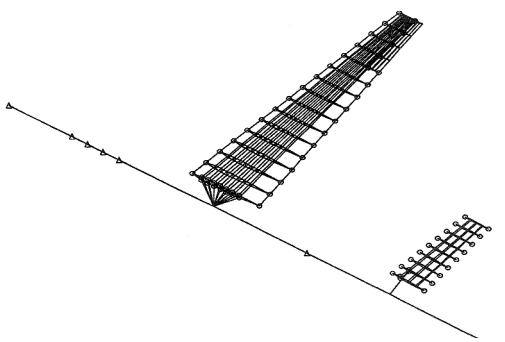

Fig. 4 Finite element model.

Table 2 Weight summary, half aircraft

Component	Weight, kg
Wing	384.6
Aileron	8.5
Elevator	98.5
Fuselage	
Structure	2700.0
Fuel	2000.0
Engine	700.0
Total	5891.6

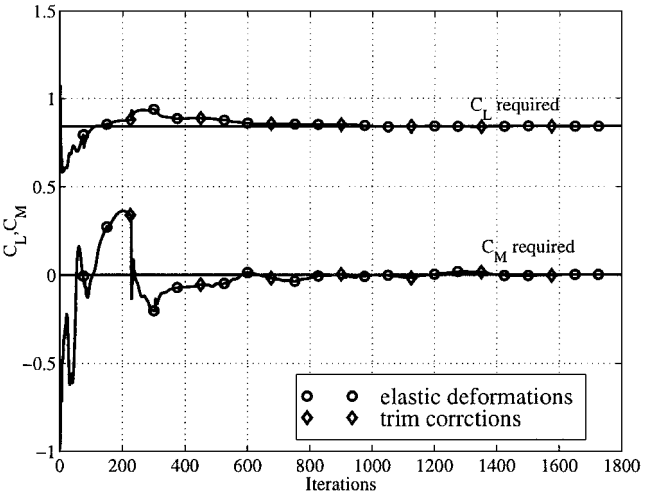

Fig. 5 Convergence history of C_L and C_M during trim analysis of a 3-g pull-up maneuver at Mach 0.85.

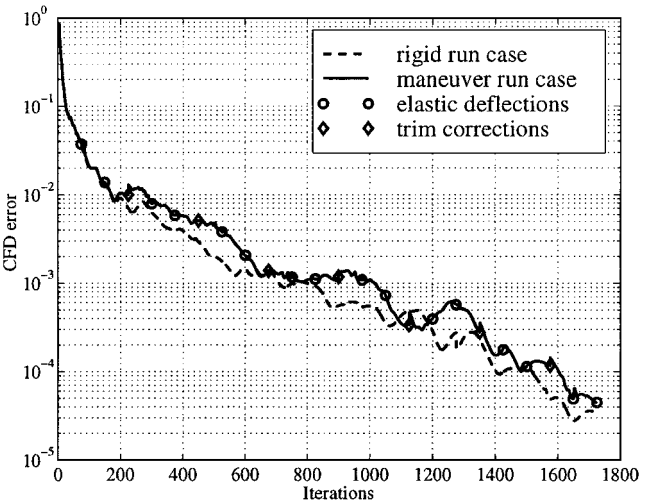

Fig. 6 Decay of the CFD error during trim analysis of a 3-g pull-up maneuver at Mach 0.85.

Maneuver Load Analysis

The following description is of a 3-g pull-up maneuver of the baseline structure, at Mach 0.85 and height of 11,000 m, which defines a pitch rate of $\dot{\theta} = (n-1)g/V = 0.066$ rad/s and which corresponds to required lift and moment coefficients of $C_L = 0.84$ and $C_M = 0$.

Figure 5 presents the convergence history of the lift and moment coefficients, indicating their approach to the required values, whereas Fig. 6 shows the convergence history of the CFD error for the maneuver run case compared to that of a regular CFD run of a rigid-shape configuration. The CFD error of Fig. 6 is defined as the error in the first flow equation, that is, the mass conservation equation, avaraged over all of the grid points. Figures 5 and 6 indicate the good convergence properties of the scheme. Reference 21

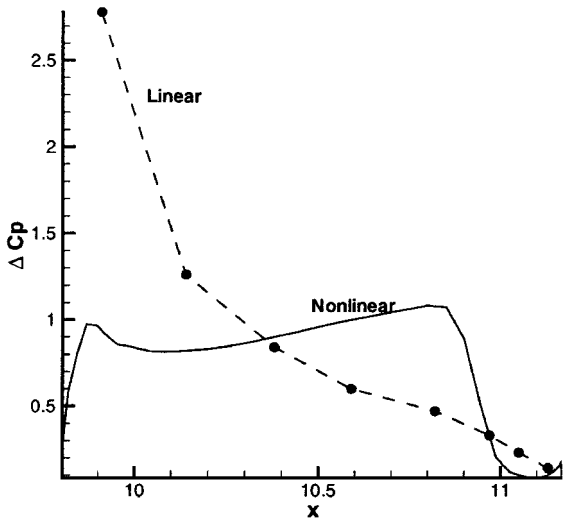

Fig. 7 Differential pressure coefficient distribution at 82% of the span.

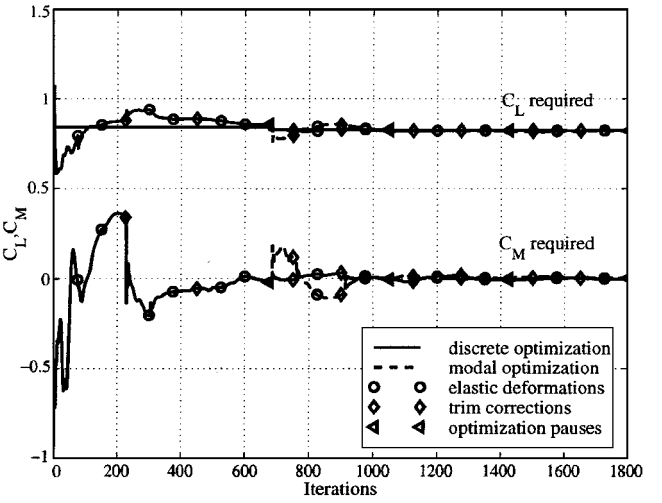

Fig. 8 Convergence history of C_L and C_M during combined trim analysis of a 3-g pull-up maneuver at Mach 0.85 and structural optimization.

includes more details on the maneuver load analysis results, plus a demonstration of the robustness of the scheme with respect to initial trim parameters and with respect to the aerodynamic derivatives that are used to trim the aircraft.

To evaluate the effects of the nonlinear modeling on the loads distribution, a second maneuver load analysis was performed, using ASTROS and its linear aerodynamic module, USSAERO.[36] Figure 7 presents the differential pressure coefficient ΔC_p distribution along a wing section at 82% of the span, which compares the linear and nonlinear values. Note that the nonlinear and linear pressure distributions significantly differ. The nonlinear chordwise center of pressure is moved aft compared to the linear one, which causes a nose-down moment and an increased sectional wash-out angle. The difference between the computed linear and nonlinear ΔC_p distributions, which is attributed to the different aerodynamic theories, has a significant effect on the structural optimization, especially on the local structural gauge distribution, as is seen in the following section.

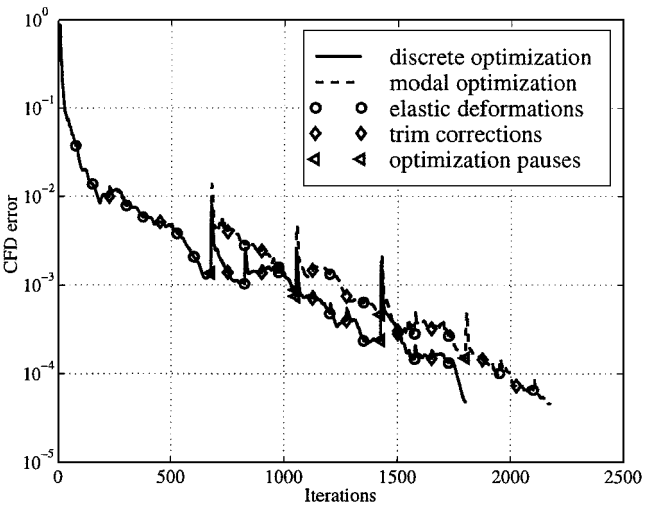

Fig. 9 Decay of the CFD error during combined trim analysis of a 3-g pull-up maneuver at Mach 0.85 and structural optimization.

Structural Design

The wing torsion box is divided into five spanwise segments. At each segment, the design variables control the thicknesses of the wing skin, the ribs, the front and rear spar webs, and the cross-sectional area of the front and rear spar-caps and the stringers, resulting in a total of 35 design variables. The torsion box is optimized for minimum weight under the following constraints.

1) The von Mises stresses are constrained by two-thirds of the material ultimate stress (280 MPa) in a symmetric 3-g pull-up maneuver at Mach 0.85, $h = 11{,}000$ m.

2) The aileron effectiveness is constrained by $\eta_r \geq 30\%$ in an antisymmetric roll maneuver at Mach 0.85, $h = 11{,}000$ m, where η_r is the aeroelastic aileron effectiveness.

The combined load-optimization process was executed by replacing every third trim correction in a maneuver load run by a structural optimization run. Optimization runs were carried out using the two approaches: 1) with the standard discrete-coordinate static aeroelastic module of ASTROS, modified to accommodate the CFD loads as a fixed set of loads to which a trim correction is added in every optimization step [according to Eq. (9)], and 2) with the modal-based option of ASTROS.

Figure 8 shows the history of convergence of the lift and moment coefficients, showing both design studies. In both cases the convergence of the aerodynamic coefficients is smooth. Until the first optimization pause, both design studies follow the same trend. Following the optimization, the plots slightly differ, where it is noted that the modal-based optimization has slightly larger fluctuations in the coefficient values.

Figure 9 shows the history of CFD-error decay of the combined maneuver-optimization run case. On return from the optimization, when the airloads are applied to the optimized structure that is less stiff, new deformations are obtained. These shape changes increase the CFD error, which then rapidly decays. The phenomenon is further amplified in the modal-based optimization due to the larger changes in the design variable values in each optimization. In the discrete-optimization run case, the total number of iterations required for convergence of the combined load-optimization run is only 20% larger than the total number of iterations required for convergence of a rigid-shape configuration (approximately 1700 iterations for the load-optimization run vs 1400 iterations for the rigid-shape run to reduce the CFD-error four orders of magnitude). In the modal-based optimization run case, the number of iterations for convergence is slightly larger (about 2000 iterations for the same reduction of the CFD error).

To evaluate the effects of nonlinear loads on the structural design, a reference optimization was performed by the standard ASTROS, with both design cases based on linear aerodynamics. The reference optimization converged within seven steps, and the variable structural weight was reduced from 284.6 to 180.0 kg. The same design task using the nonlinear maneuver loads lead to a variable structural weight of 173.9 kg. Figure 10 shows the history of weight reduction during the optimization, comparing the reference optimization with the CFD-based optimizations (discrete-coordinates and modal-based run cases). The same optimal weight was obtained by the discrete-coordinate and the modal-based optimization studies. Note that whereas in the discrete-coordinate optimization the

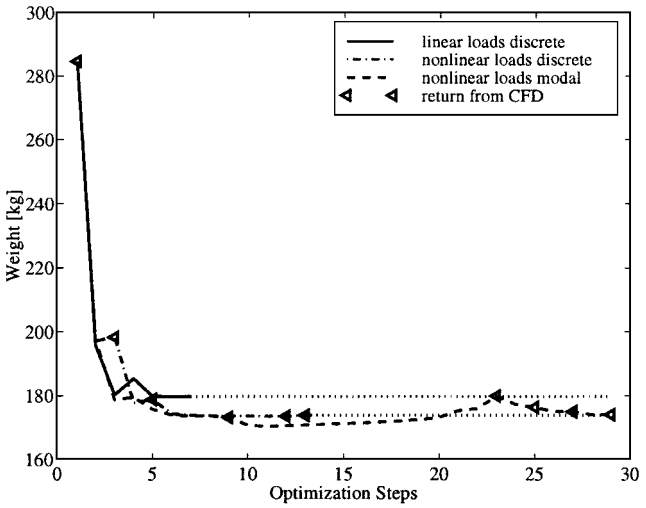

Fig. 10 Wing structure weight history.

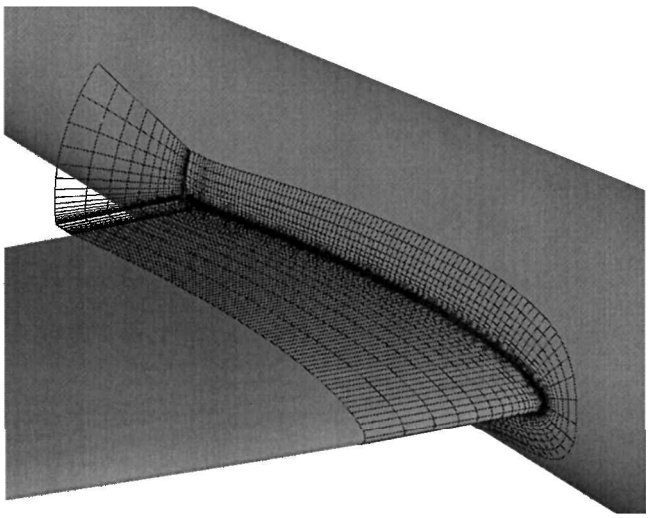

Fig. 12 Close-up of the fuselage–wing collar grid.

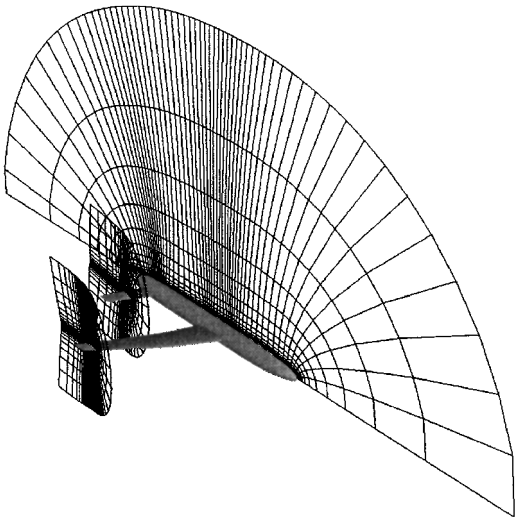

Fig. 11 Overall view of the grid system.

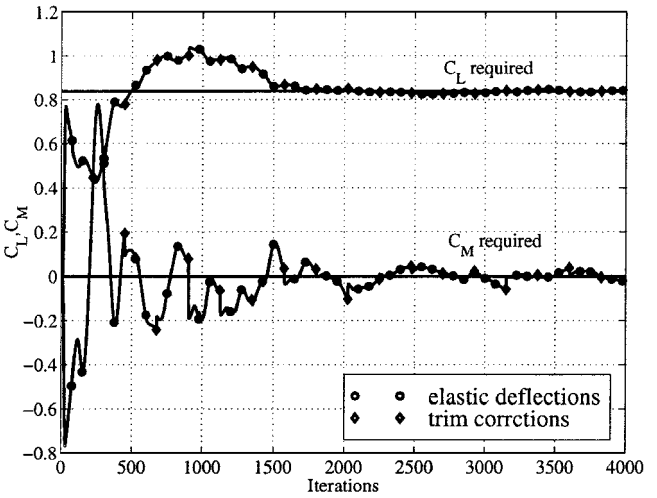

Fig. 13 Convergence history of C_L and C_M during trim analysis of a 3-g pull-up maneuver at Mach 0.85, with EZNSS.

weight was monotonically reduced, in the modal-based optimization a nonmonotonic convergence was observed. The differences in the structural weight and gauge distributions between the designs based on the linear and nonlinear loads are mainly in reducing the outboard wing weight and shifting material from the front spar to the rear spar, as discussed in Ref. 21.

Load Analysis with EZNSS

The computational mesh used for the EZNSS simulations consisted of five zones, fuselage, wing, elevator, and two collar grids, one for the fuselage–wing intersection and one for the fuselage–elevator intersection. The fuselage grid is based on an O–O type mesh. For the wing, tail, and collar grids, a C–H type grid topology is used. The entire flowfield consists of approximately 600,000 grid points. Figure 11 shows the model's complete geometry and the computational mesh of the main components. Figure 12 shows a close-up of the fuselage–wing collar grid (every other grid point in each direction is shown).

The results of the flow simulations using the EZNSS code are presented in Figs. 13–15. Figure 13 shows the convergence history of the lift and moment coefficients. Both coefficients converge to their required values, and the convergence history follows a similar behavior to the FA3DMB simulations. Figure 14 shows the convergence history of the flow simulation. The CFD error in EZNSS is defined differently than in FA3DMB, as the error in all flow equations, averaged over all of the grid points. Also shown in Fig. 14 is the convergence history of a simulation of a rigid geometry. In contrast

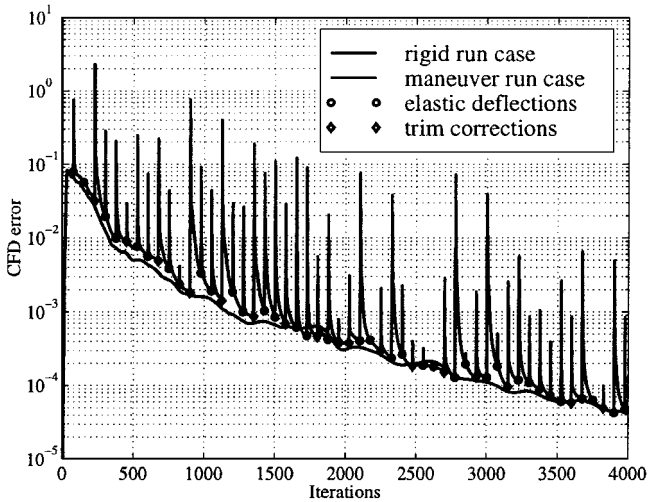

Fig. 14 Decay of the CFD error during trim analysis of a 3-g pull-up maneuver at Mach 0.85, and with EZNSS.

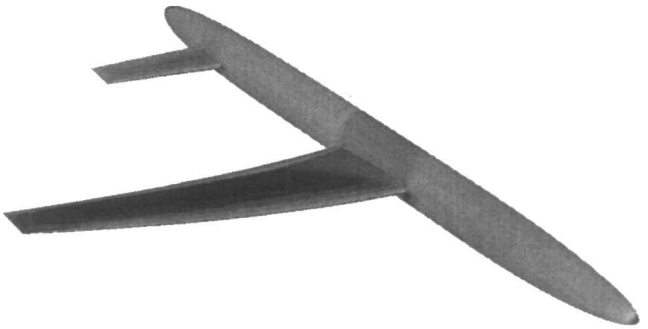

Fig. 15 Surface pressure contours at a 3-*g* pull-up maneuver at Mach 0.85, from EZNSS.

to the FA3DMB simulations, each geometry change is associated with a rather large increase of the CFD error. The large changes arise due to the Chimera overset method. Every control-surface deflection or elastic correction may change grid points in the fuselage mesh from being holes to become regular points. Because such points are far from convergence, their inclusion in the simulation contributes large values to the error terms. However, the number of these points is limited, and the implicit algorithm has fast convergence qualities. Therefore, the CFD-error values decrease quickly to the values of a rigid-shape simulation.

Figure 15 shows the converged aerodynamic pressure distribution on the aircraft surface in 3-*g* pull-up maneuver. A shock wave can be seen at approximately 85% of the chord on the upper wing surface. Another shock exists on the lower surface of the elevator. A similar image for the flow obtained using the FA3DMB code can be found in Ref. 21.

Conclusions

The paper presented an efficient methodology for structural design studies, with static aeroelastic considerations, where the aerodynamic loads are provided by a nonlinear CFD scheme. Structural optimization was performed both with the regular discrete-coordinate approach and with the modal-based option. Both cases demonstrated very good convergence properties of both the aerodynamic loads and the structural design, with the total number of CFD iterations required for convergence being almost the same as for a regular flow analysis for a rigid configuration. It was demonstrated that the use of a simplified structural modeling does not significantly affect the convergence of the combined load-optimization process. The discrete-coordinate and modal-based optimization converged to the same optimal designs, where in the modal-based optimization, a nonmonotonic convergence was observed, which in turn slightly increased the number of iterations required for convergence. For the relatively small finite element model of this study, the use of the model-based optimization does not provide any computational cost reduction; however, for larger models, the discrete-coordinate optimization must be replaced by the modal-based optimization to maintain a computationally affordable design process. Comparison between the linear and nonlinear designs showed some difference in the total weight and significant difference in the local structural gauge distribution, which indicate that accurate evaluation of the maneuver loads is important even in the early design stages.

The maneuver analysis was examined using two flow simulation schemes. The first is an explicit, finite volume scheme using a multiblock patched grid approach (FA3DMB), and the second is an implicit, finite difference code using the Chimera overset grid method (EZNSS). The EZNSS code allows for easy application of rigid-body rotations of control surfaces. The maneuver analysis exhibited good convergence properties for both codes (with different convergence patterns due to the different grid methods), which indicates that the load analysis methodology is independent of the numerical algorithm or the flow solver used.

The study establishes a framework for structural design, where some disciplines are based on nonlinear aerodynamic modeling while others are based on linear methods. The computational schemes presented are specifically designed for the study of realistic aircraft configurations, based on detailed finite element modeling and involving several design disciplines.

References

[1]Haftka, R. T., "Structural Optimization with Aeroelastic Constraints: A Survey of U.S. Applications," *International Journal of Vehicle Design*, Vol. 7, No. 3–4, 1986, pp. 381–392.

[2]Rodden, W. P., and Johnson, E. H., MSC/NASTRAN Version 68 Aeroelastic Analysis User's Guide, Macneal–Schwendler Corp., Los Angeles, 1994.

[3]Neill, D. J., Johnson, E. H., and Canfield, R. A., "ASTROS: A Multidisciplinary Automated Structural Design Tool," *Journal of Aircraft*, Vol. 27, No. 12, 1990, pp. 1021–1027.

[4]Albano, E., and Rodden, W. P., "A Doublet-Lattice Method for Calculating Lift Distributions on Oscillating Surfaces in Subsonic Flows," *AIAA Journal*, Vol. 7, No. 2, 1969, pp. 279–285.

[5]Love, M. H., "Integrated Airframe Design at the Lockheed Martin Tactical Devision," 82nd Meeting of AGARD Structures and Materials Panel, Rept. 8M, AGARD, 1996.

[6]Whitlow, W., Jr., and Bennett, R. M., "Application of a Transonic Potential Flow Code to the Static Aeroelastic Analysis of Three-Dimensional Wings," *Proceedings of the 23rd Structures, Structural Dynamics, and Materials Conference*, Vol. 2, AIAA, Washington, DC, 1982, pp. 267–276.

[7]Agrell, N., and Hedman, S. G., "Calculations of Transonic Steady State Aeroelastic Effects for Canard Airplane," *Proceedings of the 13th Congress of the International Council of the Aeronautical Sciences*, AIAA, New York, 1982, pp. 59–66.

[8]Pittman, J. L., and Giles, G. L., "Combined Nonlinear Aerodynamic and Structural Method for the Aeroelastic Design of a Three-Dimensional Wing in Supersonic Flow," *Proceedings of the Applied Aerodynamics Conference*, AIAA, Washington, DC, 1986, pp. 36–44.

[9]Tatum, K. E., and Giles, G. L., "Integrating Nonlinear Aerodynamic and Structural Analysis for a Complete Fighter Configuration," *Journal of Aircraft*, Vol. 25, No. 12, 1988, pp. 1150–1156; also AIAA Paper 87-2863, 1987.

[10]Vinh, L., Edwards, J. W., Seidel, D. A., and Batina, J. T., "Transonic Stability and Control of Aircraft Using CFD Methods," *Proceedings of the AIAA Atmospheric Flight Mechanics Conference*, AIAA, Washington, DC, 1988, pp. 394–404.

[11]Batina, J. T., Seidel, D. A., Bland, S. R., and Bennet, R. M., "Unsteady Transonic Flow Calculations for Realistic Aircraft Configurations," *Journal of Aircraft*, Vol. 26, No. 1, 1989, pp. 21–28.

[12]Schuster, D. M., Vadyak, J., and Atta, E., "Static Aeroelastic Analysis of Fighter Aircraft Using a Three-Dimensional Navier–Stokes Algorithm," *Journal of Aircraft*, Vol. 27, No. 5, 1990, pp. 820–825.

[13]Guruswamy, G. P., "Coupled Finite-Difference/Finite-Element Approach for Wing-Body Aeroelasticity," *Proceedings of the 4th Symposium on Multidisciplinary Analysis and Optimization*, AIAA, Washington, DC, 1992, pp. 1–12.

[14]Guruswamy, G. P., and Byun, C., "Direct Coupling of Euler Flow Equations with Plate Finite Element Structures," *AIAA Journal*, Vol. 33, No. 2, 1995, pp. 375–377.

[15]Appa, K., Argyris, J., and Guruswamy, G. P., "Aircraft Dynamics and Loads Computations Using CFD Methods," *Proceedings of the 37th Structures, Structural Dynamics, and Materials Conference*, AIAA, Reston, VA, 1996, pp. 215–220.

[16]Kapania, R. K., Bhardwaj, M. K., Reichenbach, E., and Guruswamy, G. P., "Aeroelastic Analysis of Modern Complex Wings," *Proceedings of the 6th Symposium on Multidisciplinary Analysis and Optimization*, AIAA, Reston, VA, 1996, pp. 258–265.

[17]Guruswamy, G. P., and Tu, E. L., "Navier–Stokes Computations on Flexible Advanced Transport Wings in Transonic Regime," *Journal of Aircraft*, Vol. 33, No. 3, 1996, pp. 576–581.

[18]Byun, C., and Guruswamy, G. P., "A Parallel, Multi-Block, Moving Grid Method for Aeroelastic Applications on Full Aircraft," *Proceedings of the 7th Symposium on Multidisciplinary Analysis and Optimization*, AIAA, Reston, VA, 1998, pp. 570–580.

[19]Karpel, M., Yaniv, S., and Livshits, D. S., "Integrated Solution for Computational Static Aeroelastic Problems," *Journal of Spacecraft and Rockets*, Vol. 35, No. 5, 1998, pp. 612–618; also AIAA Paper 96-4012, 1996.

[20]Raveh, D. E., Karpel, M., and Yaniv, S., "Nonlinear Design Loads for Maneuvering Elastic Aircraft," *Journal of Aircraft*, Vol. 37, No. 2, 2000, pp. 313–318.

[21]Raveh, D. E., and Karpel, M., "Structural Optimization of Flight Vehicles with Computational-Fluid-Dynamics-Based Maneuver Loads," *Journal of Aircraft*, Vol. 36, No. 6, 1999, pp. 1007–1015.

[22]Karpel, M., and Brainin, L., "Stress Considerations in Reduced-Size Aeroelastic Optimization," *AIAA Journal*, Vol. 33, No. 4, 1995, pp. 722–726.

[23]Karpel, M., Moulin, B., and Love, M. H., "Structural Optimization with Stress and Aeroelastic Constraints Using Expandable Modal Basis," *Proceedings of the 39th Structures, Structural Dynamics, and Materials Conference*, AIAA, Reston, VA, 1998, pp. 1460–1468.

[24]Yaniv, S., "Navier–Stokes Calculations for Rotating Configurations: Implementation for Rockets," *Journal of Spacecraft and Rockets*, Vol. 33, No. 5, 1996, pp. 756–758.

[25]Jameson, A., Schmidt, W., and Turkel, E., "Numerical Solution of the Euler Equations by Finite Volume Methods Using Runge–Kutta Time-Stepping Schemes," AIAA Paper 81-1259, 1981.

[26]Sheena, Z., and Karpel, M., "Static Aeroelastic Analysis Using Aircraft Vibration Modes," *Proceedings of the 2nd International Symposium on Aeroelasticity and Structural Dynamics*, DGLR, Aachen, Germany, 1985, pp. 229–232.

[27]Karpel, M., and Sheena, Z., "Structural Optimization for Aeroelastic Control Effectiveness," *Journal of Aircraft*, Vol. 26, No. 8, 1989, pp. 493–495.

[28]Harder, R. L., and Desmarais, R. N., "Interpolation Using Surface Splines," *Journal of Aircraft*, Vol. 9, No. 2, 1972, pp. 189–191.

[29]Raveh, D. E., "Integrated Aero-Structural Design of Maneuvering Flexible Flight Vehicles," Ph.D. Dissertation, Faculty of Aerospace Engineering, Technion—Israel Inst. of Technology, Haifa, Israel, Feb. 1998.

[30]Benek, J. A., Buning, P. G., and Steger, J. L., "A 3-D Chimera Grid Embedding Technique," AIAA Paper 85-1523, 1985.

[31]Beam, R. M., and Warming, R. F., "An Implicit Factored Scheme for the Compressible Navier–Stokes Equations," *AIAA Journal*, Vol. 16, 1978, pp. 393–402.

[32]Steger, J. L., Ying, S. X., and Schiff L. B., "A Partially Flux-Split Algorithm for Numerical Simulation of Unsteady Viscous Flows," Workshop on Computational Fluid Dynamics, 1986.

[33]Parks, S. J., Buning, P. G., Chan, W. M., and Steger, J. L., "Collar Grids for Intersecting Geometric Components Within the Chimera Overlapped Grid Scheme," AIAA Paper 91-1587, June 1991.

[34]Neill, D. J., Herendeen, D. L., and Venkayya, V. B., *ASTROS Theoretical Manual*, Flight Dynamics Directorate, Wright Lab., Air Force Material Command, Wright–Patterson AFB, OH, May 1995, pp. 121–132.

[35]Karpel, M., "Modal-Based Enhancement of Integrated Structural Design Optimization Schemes," *Journal of Aircraft*, Vol. 35, No. 3, 1998, pp. 437–444.

[36]Woodward, F. A., "An Improved Method for the Aerodynamic Analysis of Wing–Body–Tail Configurations in Subsonic and Supersonic Flow, Part I—Theory and Applications," NASA CR-2228, May 1973.

A. Messac
Associate Editor